Simulation of collective phenomena in microswimmer suspensions

Bardfalvy, Dora

2020

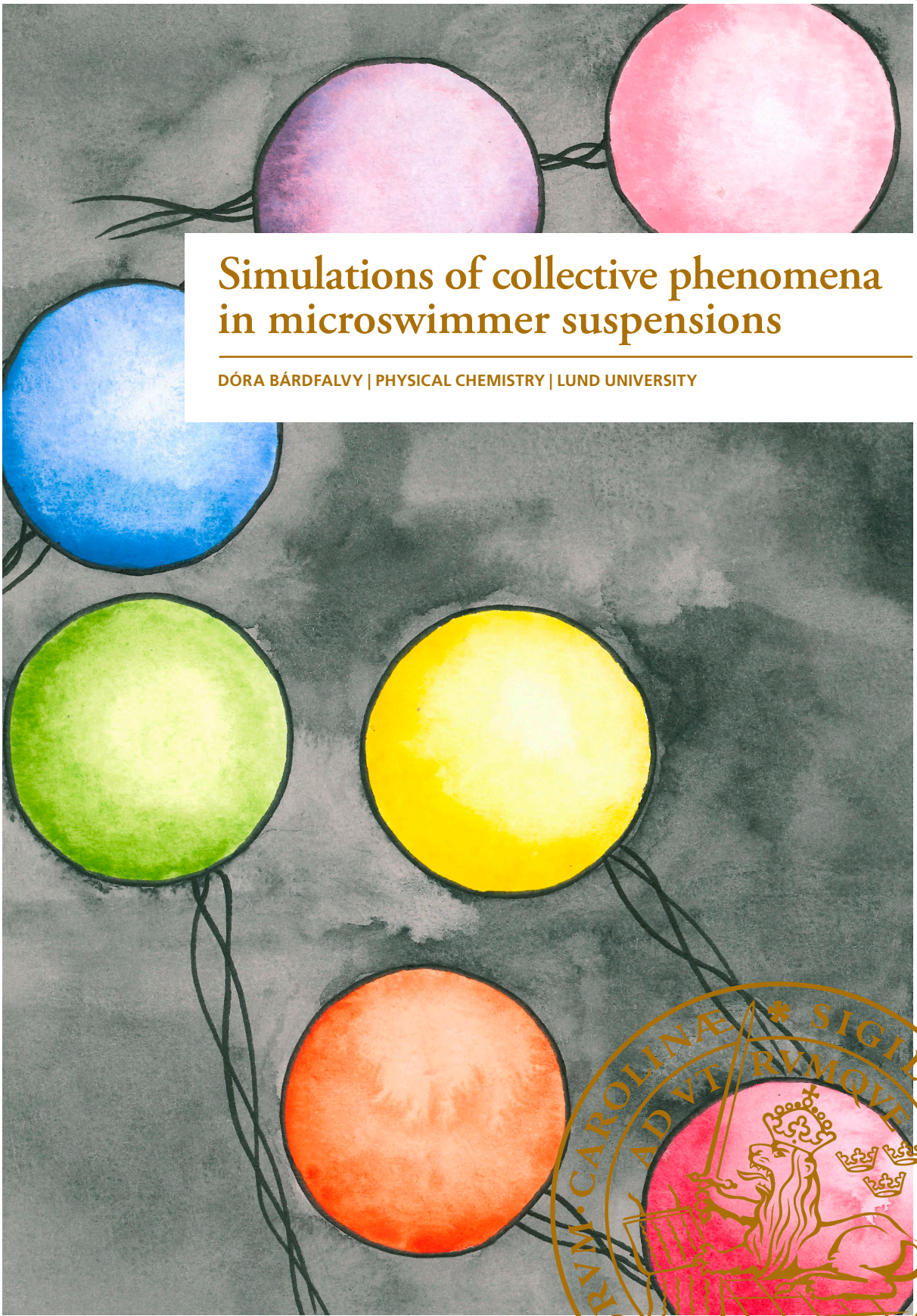

Simulations of collective phenomena in microswimmer suspensions

DÓRA BÁRDFALVY | PHYSICAL CHEMISTRY | LUND UNIVERSITY

Simulations of collective phenomena in microswimmer suspensions

Simulations of collective phenomena in microswimmer suspensions

Dóra Bárdfalvy

LUND
UNIVERSITY

DOCTORAL DISSERTATION

by due permission of the Faculty of Science, Lund University, Sweden.
To be defended on Thursday, the 17th of December 2020 at 09:15 in Lecture hall C at the Department of Chemistry, Lund University.

Faculty opponent

Prof. Dr. Gerhard Gompper
Forschungszentrum Jülich

Organization
LUND UNIVERSITY

Department of Chemistry
Box 124
SE–221 00 LUND
Sweden

Document name
DOCTORAL DISSERTATION

Date of disputation
2020-12-17

Sponsoring organization

Author(s)
Dóra Bárdfalvy

Title and subtitle
Simulations of collective phenomena in microswimmer suspensions:

Abstract

Collective motion is ubiquitous in biological and synthetic systems across many length- and timescales. On the macroscopic scale, examples include schools of fish, herds of sheep and flocks of birds. On the microscopic scale, bacteria, algae and synthetic self-propelled particles exhibit a range of collective phenomena. In suspensions of swimming bacteria, collective motion is often caused by hydrodynamic interactions between the swimmers, and is manifested as long-ranged chaotic flows, dubbed active turbulence. In this work, we study collective motion in simplified models of bacterial and algal suspensions with particle-resolved lattice Boltzmann simulations. Using an extended force dipole as a minimal model for a microswimmer, we have been able to study large systems, containing up to 3×10^6 particles, and to capture information about large-scale collective behaviours. We have studied four separate aspects of collective motion in microswimmer suspensions. First, we performed unprecedentedly large simulations of 3-dimensional active suspensions to test predictions from kinetic theory about the transition to active turbulence and characterize the ensuing turbulent state. The focus was then turned to the effects of swimming velocity on the transition to active turbulence of pusher suspensions. In nature, front- and rear-actuated microswimmers (so called pushers and pullers, respectively) coexist, which motivated us to study how the presence of pullers in the suspension changes the collective behaviour of pushers. Finally, motivated by the fact that most experiments are performed in 2-dimensional geometries, we also investigated and characterized the collective phenomena in a quasi-2-dimensional system, finding important qualitative differences compared to unbounded suspensions.

Key words
Lattice Boltzmann, microswimmers, active matter, collective motion

Classification system and/or index terms (if any)

Supplementary bibliographical information

Language
English

ISSN and key title

ISBN
978-91-7422-770-3 (print)
978-91-7422-771-0 (pdf)

Recipient's notes

Number of pages
108

Price

Security classification

Simulations of collective phenomena in microswimmer suspensions

by Dóra Bárdfalvy

LUND
UNIVERSITY

This doctoral thesis is constructed as a summary of research papers and consists of two parts. An introductory text puts the research work into context and summarizes the main conclusions of the papers. Then, the research publications themselves are reproduced. The research papers may either have been already published or are manuscripts at various stages.

Cover: Microswimmers by Dóra Bárdfalvy

Faculty of Science, Department of Chemistry, Division of Physical Chemistry

ISBN: 978-91-7422-770-3 (print)
ISBN: 978-91-7422-771-0 (pdf)

Printed in Sweden by Media-Tryck, Lund University, Lund 2020

Media-Tryck is a Nordic Swan Ecolabel certified provider of printed material. Read more about our environmental work at www.mediatryck.lu.se

MADE IN SWEDEN

Abstract

Collective motion is ubiquitous in biological and synthetic systems across many length- and timescales. On the macroscopic scale, examples include schools of fish, herds of sheep and flocks of birds. On the microscopic scale, bacteria, algae and synthetic self-propelled particles exhibit a range of collective phenomena. In suspensions of swimming bacteria, collective motion is often caused by hydrodynamic interactions between the swimmers, and is manifested as long-ranged chaotic flows, dubbed active turbulence. In this work, we study collective motion in simplified models of bacterial and algal suspensions with particle-resolved lattice Boltzmann simulations. Using an extended force dipole as a minimal model for a microswimmer, we have been able to study large systems, containing up to 3×10^6 particles, and to capture information about large-scale collective behaviours. We have studied four separate aspects of collective motion in microswimmer suspensions. First, we performed unprecedentedly large simulations of 3-dimensional active suspensions to test predictions from kinetic theory about the transition to active turbulence and characterize the ensuing turbulent state. The focus was then turned to the effects of swimming velocity on the transition to active turbulence of pusher suspensions. In nature, front- and rear-actuated microswimmers (so called pushers and pullers, respectively) coexist, which motivated us to study how the presence of pullers in the suspension changes the collective behaviour of pushers. Finally, motivated by the fact that most experiments are performed in 2-dimensional geometries, we also investigated and characterized the collective phenomena in a quasi-2-dimensional system, finding important qualitative differences compared to unbounded suspensions.

Table of Contents

Acknowledgements

This was one of the most difficult parts for me to write in this thesis. I have been lucky enough to interact with both the physical and theoretical chemistry divisions, which means that now I have so many people to thank. I cannot write all the names because this acknowledgement would be too long. I collected so many memories during the last few years I spent here: so many friendships, laughs, unforgettable discussions during good and difficult times, and fun during choir rehearsals.

Helena and Maria Lövgren, thank you for your patience, that I could come to you with all sorts of questions. Likewise, Maria Södergren and Chris, I could always count on your help if I had problems in the lab while teaching and in various other occasions when I had technical problems. Paula, thank you for all your help with this thesis, your comments and suggestions were very useful. Dear Kristin, thank you so much for the huge help with the figures! My papers and this thesis look much better because of you.

Alex, Viktor and Cesare, thank you for all the scientific and non-scientific discussions on several occasions, I learnt a lot. I had so much fun during our meetings and during dinners while drinking beer (or whisky) or reading the chat group. I am proud and happy to collaborate with you!

Past and present group members, Shan, Yoshimi, André, Jason, and Henrik, thank you for all the fun times and nice discussions either in the office, during lunch or fika, or while traveling.

I also had three wonderful supervisors. Emma, thank you for all our discussions, you were always interested in my project and development. I could also talk to you every time I had problems during teaching and you always gave me good advice. I would like to thank my other amazing supervisor, Martin. I enjoyed all the fun and nice discussions during fika and lunch. I really appreciate all your help during these years, I could just pop up in your office and you were always ready to help. Last, but definitely not least, Joakim. I don't even know where to start. You were always there so support me from the first days until now. Whatever problem I had, I know I could always come to you and you always tried to help. Maybe it was not always easy (sorry), but I think we managed really well and I enjoyed working with you. I also enjoyed the lunches, dinners, our long walks with endless discussions (even when we almost got lost) and listening to your concerts. Thank you for everything!

Thank you so much everyone who has read this thesis, giving me feedback that has been so helpful while trying to summarize what I have done during these years.

Popular scientific summary

In many nature documentaries, one can see birds flying in big flocks, fish swimming together in schools, or sheep moving together as a herd. Moving as one big entity is often a huge advantage that makes it easier to survive: it is safer to find food and water if one is shielded in a crowd, hiding away from predators. Similar behaviour can be observed if one looks into a microscope to study bacteria and algae. These microorganisms are able to swim on their own by propelling themselves with flagella connected to their cell bodies. Together, such *microswimmers* can swim faster with coherent motion over much larger distances than the individual bacterium. This is called active turbulence, because if one looks at a video of such a suspension of bacteria, they will swim together in a jet-like motion. The properties and origin of such a collective behaviour of the bacteria is thus an interesting and important phenomenon to study, and that is the objective of this thesis.

My work focuses on two different types of microswimmers. One has flagella in the back and propels itself by performing a circular motion with the flagella, it is called a *pusher*. *Puller* microswimmers, on the other hand, have two flagella in the front, moving in a breaststroke-like pattern. Good examples of pushers and pullers are *E. coli* bacteria and the *Chlamydomonas* algae respectively. Active turbulence occurs only in suspensions of pusher microorganisms, because they can mutually reorient themselves, resulting in the ability of pushers swimming side-by-side, which is not observed in the case of pullers.

To understand how the properties of the individual microswimmers can lead to different collective behaviour, computer simulations are a good tool. Using different models for the microswimmers, as well as for their environment, one can mimic different experimental situations, but also understand how they would behave in environments which might not be easy to realise in an experiment. For example, confining their motion to a thin layer of fluid, which is often done in experiments, or letting them move without any boundaries. Computer simulations thus enable us to study microswimmers in detail, and to see what macroscopic properties different models would predict.

In this thesis, I studied the hydrodynamic interactions between different microswimmers mediated by the fluid in which they move, and how this can result in a collective motion. Using a rather simple model for the swimmers, we could capture some important phenomena that occur when bacteria swim together. We could see the active turbulence in pusher suspensions, and also how the presence of pullers in a pusher suspension changes the dynamics. Confining the microswimmers to a two-dimensional layer, we also observed clustering of pullers. These are all phenomena that have been

observed experimentally, which is an indication of that the model used in the simulations includes the important features to understand what has been observed in experiments.

List of Publications

This thesis is based on the following publications, referred to by their Roman numerals:

I **Particle-resolved lattice Boltzmann simulations of 3-dimensional active turbulence**

D. Bárdfalvy, H. Nordanger, C. Nardini, A. Morozov, J. Stenhammar
Soft Matter **2019**, 15, 7747

II **The effect of swimming speed on the collective motion in suspensions of pusher microswimmers**

D. Bárdfalvy, V. Škultéty, C. Nardini, A. Morozov, J. Stenhammar
Manuscript

III **Symmetric mixtures of pusher and puller microswimmers behave as noninteracting suspensions**

D. Bárdfalvy, S. Anjum, C. Nardini, A. Morozov, J. Stenhammar
Phys. Rev. Lett. **2020**, 125, 018003

IV **On the effect of confinement on collective behaviour in microswimmer suspensions**

D. Bárdfalvy, V. Škultéty, C. Nardini, A. Morozov, J. Stenhammar
Manuscript

Author Contributions

Paper I: Particle-resolved lattice Boltzmann simulations of 3-dimensional active turbulence

DB performed the simulations and analysis, while AM and CN performed the theoretical calculations. DB wrote the manuscript with input from the co-authors.

Paper II: The effect of swimming speed on the collective motion in suspensions of pusher microswimmers

DB performed the simulations and analysis, DB and JS wrote the manuscript with input from the co-authors.

Paper III: Symmetric mixtures of pusher and puller microswimmers behave as non-interacting suspensions

SA performed the simulations under the supervision of DB and JS, CN and AM performed the theoretical calculations. SA and DB performed the analysis, and JS wrote the manuscript with input from the co-authors.

Paper IV: On the effect of confinement on collective behaviour in microswimmer suspensions

DB performed the simulations and analysis with the input from JS, VS and AM. DB and JS wrote the manuscript with input from the co-authors.

Nomenclature

Latin alphabet

a	Effective body radius
$\mathbf{c}$	Velocity vector
c_s	Speed of sound
$c(R)$	Spatial correlation function of the fluid velocity
$c(t)$	Temporal correlation function of the fluid velocity
d_r	Rotational diffusion coefficient
D	Centre of mass diffusion coefficient
$\mathbf{e}$	Propulsion direction
$\mathbf{E}$	Rate of strain tensor
f	Phase-space density
f_i	Single-particle distribution function
f^{eq}	Equilibrium distribution function
$\mathbf{F}$	Force
h	Height of fluid film
$\mathbb{I}$	Unit tensor
k_c	Critical wavevector
l	Swimmer length
l_p	Average persistence length of the microswimmers
L	Side-length of the simulation box
ΔL	Lattice spacing
n	Number density of microswimmers
n_c	Critical density
N	Number of microswimmers
p	Pressure
$\mathbf{p}_i$	Orientation of swimmer i
P	Polar order parameter
P_n	n-th Legendre polynomial
$\mathbf{r}_i$	Position of swimmer i
$\mathbf{r}$	Position
Re	Reynolds number
S	Nematic order parameter
t	Time

T	Relaxation time
$\mathbf{u}$	Momentum
$\mathbf{U}(\mathbf{r})$	Fluid velocity
U_{RMS}	Root-mean-square fluid velocity
v_r	Radial slip velocity
v_θ	Tangential slip velocity
v_s	Swimming speed
$\mathbf{V}$	Vorticity tensor
w_i	Weights of the velocity set
$\mathbf{W}$	Flow field generated by the flagellum

Greek alphabet

γ	Shape parameter
Δ	Ratio of the microswimmer density and the critical density
θ	Angle
κ	Dipole strength
κ_n	Nondimensionalized dipole strength
λ	Tumbling frequency
Λ	Non-dimensional microswimmer persistence length
μ	Dynamic viscosity
ξ	Characteristic lengthscale
ρ	Density
τ	Characteristic timescale
χ	Fraction of pullers
Ψ	Probability density
ω	Vorticity
Ω	Collision operator

1 Introduction

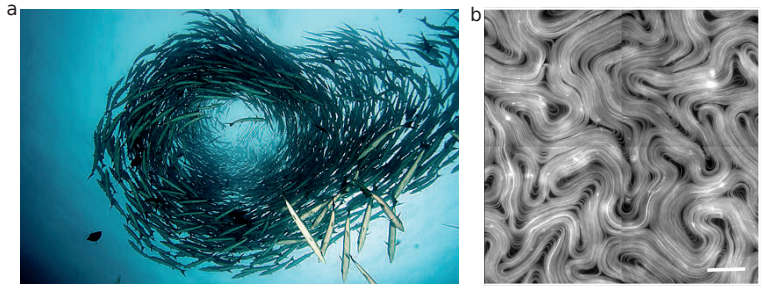

Figure 1.1 (a) A school of barracudas[1] and (b) collective motion of microtubules mixed with kinesin. The scale bar represents $100\ \mu\mathrm{m}$.[2]

Most aqueous environments are full of microorganisms, like algae in sea and lake water and bacteria in the human body. Some of them can actively propel themselves, because their survival depends on being able to effectively move around to find food and better living conditions. This thesis will highlight some of the phenomena arising from the swimming of microorganisms, and from the forces they apply to their environment when doing so.

1.1 Active matter

Active matter is a research field at the boundary between physics, biology and chemistry, which studies particles, biological or synthetic, that are able to extract energy from the environment and use that to perform thermodynamic work, thus driving them out of thermodynamic equilibrium.[3-5] This work, usually in the form of self-propulsion, often leads to large-scale collective motion. Macroscopic examples of such collective motion include bird flocks[6] and schools of fish (Fig. 1.1a), while examples of collective motion at smaller scales include motility-induced clustering,[7] enhanced diffusion of passive tracer particles in active suspensions,[8-11] and bacterial or active turbulence. This denotes large scale flows in bacterial suspensions at high enough densities, with fluid flows significantly faster than the swimming velocity of an individual bacterium.[12-16] Another experimental example of active turbulence are the swirls created by microtubules mixed with motor proteins, shown in Fig. 1.1b.

Various theoretical models have been used to describe these experimental phenomena, starting from basic physical principles. One of the earliest and most widely studied model of active matter is the Vicsek model,[17] which describes the dynamics of flocking using self-propelled particles with a simple polar alignment rule. In spite of its simplicity, the Vicsek model has proven successful in qualitatively describing the collective behaviour of groups of animals, like the flocking of birds. Another well-studied mi-

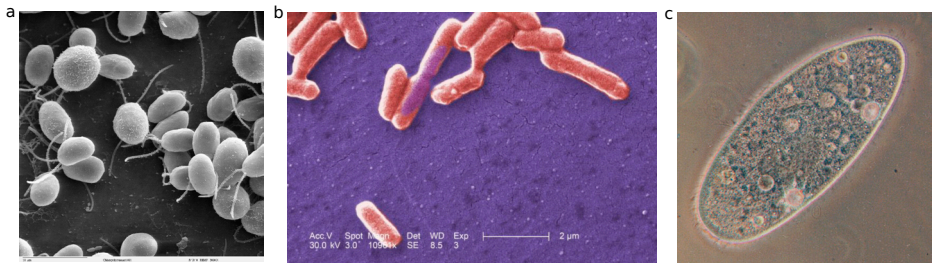

Figure 1.2 Some examples of biological microswimmers: (a) ***Chlamydomonas*** [19] (flagellated puller alga), (b) ***E. coli*** [20] (flagellated pusher bacterium), and (c) ***Paramecium*** [21] (ciliated eukaryote).

nimal active matter model considers suspensions of spherical self-propelled particles with isotropic repulsive interactions, so-called active Brownian particles. As the density increases, their local velocity decreases due to collisions, resulting in an instability leading to separation into dense and dilute phases, dubbed motility-induced phase separation.[18] Both of these models describe particles that move by exchanging momentum with a solid substrate, and thus fall into a class called "dry" active matter.

Microscopic active particles that instead move by swimming through a momentum-conserving fluid fall into the class of wet active matter, or *microswimmers*. Since they are self-propelled, each swimmer is force- and torque-free.[3,22] Synthetic swimmers can have very different shapes and sizes, typically ranging from micrometers to centimeters. The shapes are also varied between platelets, rods, spheres and helices.[22] A common experimental example of synthetic microswimmers are self-propelled Janus particles,[7,23,24] which have two parts with different physical or chemical properties. The asymmetric structure enables the two hemispheres of the particles to react in different ways to their environment, resulting in self-propulsion. The mechanism for this can be a chemical reaction catalysed by the particle surface or the local heating of the particle, generating motion through thermophoresis or local demixing of the solvent.[22] Biological microswimmers, in contrast, typically swim by deforming (part of) their bodies. Many species of microorganisms use a collection of flagella to propel themselves.[3,25] Spermatozoa and *Caulobacter* have only a single flagellum attached to the body by a rotary motor that turns it,[3] while the alga *Chlamydomonas* (Fig. 1.2a) has two head-mounted flagella that beat synchronously, resulting in a breaststroke-like swimming gait.[26] *Escherichia coli* (Fig. 1.2b) and *Salmonella typhimurium* have a bundle of side- and rear-mounted helical flagella that rotate as a bundle to propel the cells.[27] When they want to change direction, they unbundle the flagella by rotating them counterclockwise, leading to a so-called "tumble". In ciliated species, like *Paramecium* (Fig. 1.2c) and other protozoa, the whole surface of the organism is covered by a carpet of cilia, which beat in an organized wave-like pattern, mediated

by hydrodynamic interactions, leading to self-propulsion.[28] In wet active matter, hydrodynamic interactions are dominating and as a result of flow fields of the individual microorganisms, pusher bacteria can mutually reorient resulting in collective motion.

1.2 Goals of this thesis

In this thesis, I will study several aspects of hydrodynamically induced collective phenomena in model microswimmer suspensions, in particular active turbulence. The main goals of this work are:

- To characterize the turbulent state and the transition from disordered swimming to bacterial turbulence in 3-dimensional pusher suspensions, and compare the results to analytical predictions
- To investigate the effect of varying swimming speed on the transition to bacterial turbulence
- To study collective motion in binary mixtures of pushers and pullers
- To investigate the effect of 2-dimensional confinement on the collective behaviour in pusher and puller suspensions.

2 Swimming at low Reynolds numbers

2.1 Navier–Stokes equations

In the simulations in this thesis, the effect of hydrodynamic interactions between microswimmers is studied, where the fluid is described by the Navier–Stokes equations for an incompressible fluid. These describe the velocity $\mathbf{U}(\mathbf{r}, t)$ of a fluid with a density ρ and viscosity a μ [29,30]

$$\rho \left\{ \frac{\partial \mathbf{U}}{\partial t} + (\mathbf{U} \cdot \nabla)\mathbf{U} \right\} = -\nabla p + \mu \nabla^2 \mathbf{U} + \mathbf{F}, \qquad \nabla \cdot \mathbf{U} = 0 \tag{2.1}$$

where p is the pressure and $\mathbf{F}$ contains all forces applied to the fluid. The left-hand side of the equation describes the effects of inertia, whereas the right-hand side contains the effect of viscous and external forces. The ratio of the inertial and viscous contributions is commonly expressed as the dimensionless *Reynolds number*:

$$\mathrm{Re} = \frac{\text{Inertial forces}}{\text{Viscous forces}} = \frac{\rho U l}{\mu} \tag{2.2}$$

where l and U represent the typical length and velocity scales of the problem in question. The typical size of a bacterium is a few micrometers and the velocity is around $10\ \mu$m/s, resulting in $\mathrm{Re} \approx 10^{-4}$ in water. [30] A Reynolds number significantly below unity means that the inertial forces are negligible, which is clearly the case for microswimmers. In contrast, larger animals swim at Reynolds numbers where inertial forces dominate: For small fish $\mathrm{Re} \approx 10^2$ and for humans $\mathrm{Re} \approx 10^4$. [31] As we will see below, this difference has important implications for what swimming mechanisms are useful at the microscale compared to those adopted by macroscopic animals.

One consequence of the low Reynolds number dynamics of microswimmers is the *scallop theorem*, [31,32] which states that, if a low-Re swimmer deforms its body periodically in a way that is identical when viewed forward and backward in time, its net motion will be zero. Importantly, this applies independently of the *rate* of the transformations, so that performing the same deformation forward and backward at different speeds cannot lead to net propulsion. It is called the *scallop theorem* since scallops swim by rapidly opening their two shells and then closing them at a slower speed. Thus, they can only propel themselves thanks to inertial forces, while the same swimming gait would not work for a microswimmer.

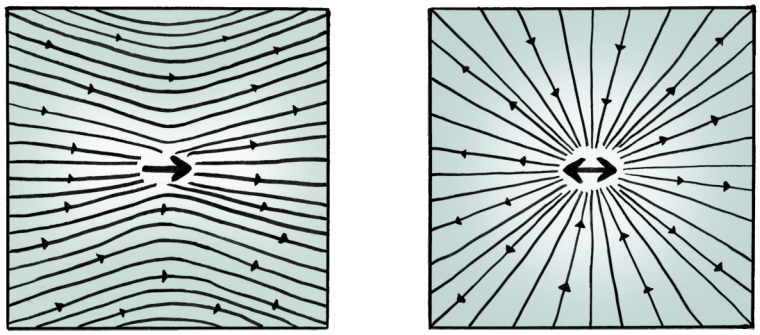

Figure 2.1 Stream lines of the flow field around a force monopole (left) and a force dipole (right).

2.2 Flow singularities

In the zero Reynolds number limit, we can neglect the inertial terms in the Navier–Stokes equations, leading instead to the Stokes equations:[30]

$$\nabla p = \mu \nabla^2 \mathbf{U} + \mathbf{F}, \qquad \nabla \cdot \mathbf{U} = 0. \tag{2.3}$$

In comparison to the full Navier–Stokes equations, the Stokes equations are far less complex to solve. Due to their linearity, even fairly complex flow fields can thus be described using a superposition of flow singularities, corresponding to the different terms in a multipole expansion of the flow field. Performing a multipole expansion, one arrives at the leading term, which is a Stokeslet (a monopole), which describes the flow field due to a point force $F = F_p \delta(r)$ applied to the fluid at the origin:

$$\mathbf{U} = \frac{\mathbf{F}}{8\pi\mu} \cdot \left(\frac{\mathbb{I}}{r} + \frac{\mathbf{rr}}{r^3} \right) \tag{2.4}$$

where $r = |\mathbf{r}|$ and $\mathbb{I}$ is the identity matrix. The flow field is shown in Fig. 2.1a and decays as $1/r$, as can be seen from Eq. 2.4. To approximately describe the flow field around a microswimmer, we need to proceed to the second term in the multipole expansion, since the swimmers are force free. The second term in the expansion is the force dipole. For a point dipole with dipole strength κ, the dipolar flow field is given

by

$$\mathbf{U} = \frac{\kappa}{8\pi r^3}(3\cos^2\theta - 1)\mathbf{r} \tag{2.5}$$

where θ is the angle and the flow field decays as $1/r^2$ (Fig. 2.1 on the right). For an extended force dipole consisting of two forces $\pm F$ separated by a length l, κ is given by

$$\kappa = \pm\frac{Fl}{\mu} \tag{2.6}$$

where κ, depending on the relative orientation of the two forces, can be either positive (pointing away) or negative (pointing towards each other). Translated into microswimmer language, these two cases correspond to microswimmers that are either rear-actuated ("pushers", $\kappa > 0$) or front-actuated microswimmers ("pullers", $\kappa < 0$). Most swimming bacteria are pushers, while the alga *Chlamydomonas* is commonly used as a model puller organism, although it actually switches between pusher and puller sequences over a period of its beating cycle.[33,34] As we will see below, this nature of the swimmer flow field (pusher or puller) has large implications on collective behaviour.

3 Collective motion in wet active matter

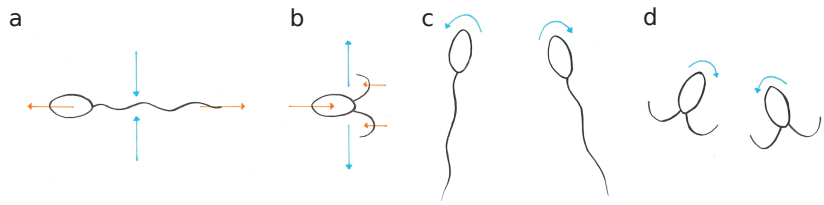

Figure 3.1 Schematic flow field around (a) a pusher and (b) a puller. (c) The hydrodynamic alignment between two pushers and (d) the corresponding antialignment between two pullers.

3.1 Hydrodynamic interactions of microswimmers

The hydrodynamic interactions between swimming cells are important already at low microswimmer density because they are long ranged.[12,35-37] We already established in Chapter 2.2 that a microswimmer is force-free and the flow field around it is dipolar to leading order and thus decays as $1/r^2$. We also established that there are two types of microswimmers depending on the sign of the dipole strength: pushers and pullers. Due to the orientation of their force dipoles, pushers expel fluid along their main axis and attracts the fluid perpendicular to it, while pullers do the opposite (Fig. 3.1 a and b). This results in a hydrodynamic attraction between two pushers side-by-side and a repulsion between two pullers in the same configuration.[3,38] The other, and more important effect of the dipolar flow field is the mutual reorientation of the microswimmers due to their velocity gradients. As seen in Fig. 3.1c, when two pushers come close to each other, they will mutually reorient into a configuration where they swim side-by-side. In contrast, pullers tend to reorient towards a $180°$ angle, thus destabilizing the side-by-side configuration (Fig. 3.1d).

A biologically important phenomenon is a microswimmer near a boundary. Due to the hydrodynamic interactions with the wall, this configuration will affect the dynamics of microswimmers in different ways depending on their propulsion mechanism. For example, *E. coli* or spermatozoa swim in a circular motion parallel to the wall, because of the torque from their rotating flagella. Due to their dipolar flow fields, pusher swimmers tend to align with the surface, just as it would do with another pusher, while pullers will swim directly towards the wall and therefore accumulate at the surface.[39-41]

3.2 Theoretical models of active turbulence

A detailed description of active matter systems and their complex behaviour is challenging due to the many factors involved, like the cell shape and the nature of its flow field as well as other, non-hydrodynamic interactions. As mentioned above, active turbulence is a phenomenon, where pusher microorganisms exhibit large-scale, turbulent-like, coherent motion.[42-44] This collective motion occurs when the density is high enough. To theoretically describe these systems, multiple models have been suggested. One successful model is called active nematics, which describes the active suspension using continuum equations.[4,45,46] The starting point of these models is a set of equations describing equilibrium nematic liquid crystals as a base. The velocity field of the surrounding fluid is then described by coupling the liquid crystal equations to the Stokes equation, including an extra term due to the "active stress" caused by the microswimmers. Again, the sign of this term indicates if the activity is pusher- or puller-like. Suitable experimental model systems reminiscent of active nematics models are made of elongated, self-propelled particles, like microtubules mixed with motor proteins, other filaments or dense suspensions of elongated bacteria. Experimental examples of pushers and pullers are microtubule and kinesin suspensions,[43] as seen in Fig. 1.1b and mouse fibroblast cells,[47] respectively. In the collective state, at the boundaries of the collective region (jets) topological defects form, where the orientation of the domain changes.[48] Active nematic-type models are successful in capturing large-scale dynamics, but due to their continuum nature they are not able to describe the interactions at the lengthscale of a particle. These models assume a nematic alignment even in the absence of activity, which is absent in bacterial suspensions except for at extremely high densities.

Another approach to theoretically describe microswimmer suspensions is kinetic theory. Such a theory starts directly from the equations of motion, describing each swimmer as a point dipole acting on the surrounding fluid.[36,49-52] The swimmer is described by the dipole strength, which also determines if it is a pusher or a puller. By using the Fokker–Planck equation, the equations of motion of the individual swimmers can be recast as an equation for the continuum probability density $\Psi(\mathbf{r}, \mathbf{p}, t)$ of microswimmers: [53]

$$\frac{\partial \Psi}{\partial t} = -\nabla_{\mathbf{r}} \cdot (\dot{\mathbf{r}}\Psi) - \nabla_{\mathbf{p}} \cdot (\dot{\mathbf{p}}\Psi) \tag{3.1}$$

The flux in particle position, $\dot{\mathbf{r}}$, depends on the swimming velocity and the local fluid velocity, as well as on the translational diffusion, while the orientational velocity is modelled using Jeffery's equation[54] including thermal rotational diffusion[50]

$$\dot{\mathbf{r}} = v_s \mathbf{p} + \mathbf{U}(\mathbf{r}) - D\nabla_{\mathbf{r}}(\ln \Psi) \tag{3.2}$$

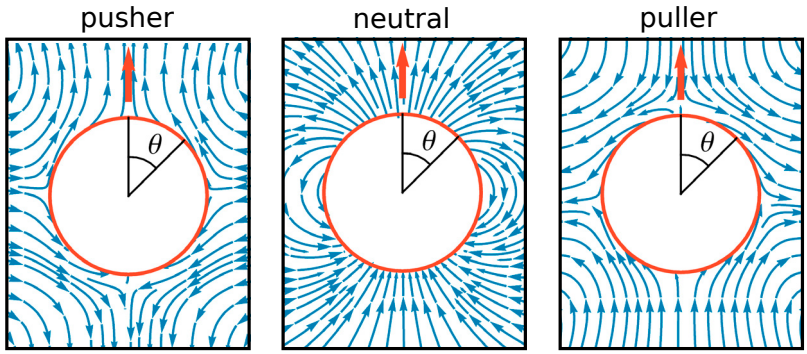

Figure 3.2 Flow fields around a pusher squirmer[55] (left), neutral squirmer[56] (middle), and puller squirmer[57] (right).

$$\dot{\mathbf{p}} = (\mathbb{I} - \mathbf{pp}) \cdot [(\gamma \mathbf{E} + \mathbf{V}) \cdot \mathbf{p} - d_r \nabla_{\mathbf{p}} (\ln \Psi)] \tag{3.3}$$

where D and d_r are the centre of mass and rotary diffusion coefficients, $\mathbb{I}$ is the identity matrix, $\mathbf{E}$ and $\mathbf{V}$ are the fluid rate of strain and vorticity tensors, and γ is the shape parameter, with $\gamma = 0$ corresponding to a spherical swimmer and $\gamma = 1$ to an infinitely thin rod. Performing a linear stability analysis on the homogeneous and isotropic base state shows that this state is unstable for pusher suspensions, which has been interpreted as a transition to active turbulence, while puller suspensions are linearly stable at all densities. This interpretation is furthermore supported by non-linear simulations of the mean-field equation (Eq. 3.1), which shows chaotic, large-scale motion similar to what is observed in experiments.

3.3 Computational models of microswimmers

To form an intermediate link between experiments and kinetic theory, one usually performs simulations using particle-resolved microswimmer models.

Historically, the most well-studied model is the squirmer model, that was originally developed by Lighthill[58] and Blake.[59] Here, the microswimmer propels through an imposed slip velocity on its surface. It models the motion of microorganisms which propel themselves using beating cilia covering the surface, such as *Paramecium* or *Volvox*. For a spherical swimmer with axisymmetric motion, the radial and tangential

slip velocities can be written as:

$$v_r = \sum_{n=1}^{\infty} A_n P_n \left(\frac{\mathbf{p} \cdot \mathbf{r}}{a} \right) \tag{3.4}$$

$$v_\theta = \sum_{n=1}^{\infty} B_n V_n \left(\frac{\mathbf{p} \cdot \mathbf{r}}{a} \right) \tag{3.5}$$

where P_n is the n-th Legendre polynomial and V_n is defined by:

$$V_n(\cos\theta) = \frac{2}{n(n+1)} \sin\theta P_n'(\cos\theta). \tag{3.6}$$

The position vector $\mathbf{r}$ represents the centre of the particle, $\mathbf{p}$ its propulsion direction, a is the squirmer radius, and A_n and B_n are constants that characterize the motion of the swimmers. The fluid velocity is described by the Stokes equations. The ratio of B_2/B_1 determines the type of the swimmer. When it is positive, the flow-field is puller-like and if it is negative it is pusher-like, while $B_2/B_1 = 0$ corresponds to a "neutral" swimmer which has neither characteristic. The flow fields of all three types are shown in Fig. 3.2. Starting from a suspension where the swimmers are randomly distributed, but their orientations are aligned, pushers quickly decorrelate, while puller suspensions at high densities show flocking with long-ranged polar order at the lengthscale of the whole system.[60] Furthermore, it has been found that the hydrodynamic interactions suppress motility-induced phase separation (MIPS) for spherical squirmers, but using elongated swimmer bodies, the MIPS is instead enhanced if the force dipole is weak. Furthermore, pullers are more likely to cluster than neutral swimmers and pushers,[61] in two dimensions, in analogy with the results found by us and discussed in Chapter 7. In spite of the similar results obtained using two different models, squirmer collective behaviour is different from that predicted for purely dipolar swimmers, due to the more complex flow fields and the presence of excluded volume.

Another particle-based method to simulate collective motion is to use slender rod swimmers. In this, the particles have a high aspect ratio and they propel themselves with a force density imposed on half of the rod, while having a no-slip boundary on the other half. This can result in both pusher and puller dipolar flow fields, depending on the position of the imposed velocity on the particle. Using this model, one can observe a transition to active turbulence above a critical density for pusher suspensions, in accordance with the predictions from kinetic theory. This results in large-scale flows and enhanced diffusion in of passive tracer particles.[62-64] Pullers, however, do not show any bacterial turbulence, as predicted by kinetic theory.

4 Model and method

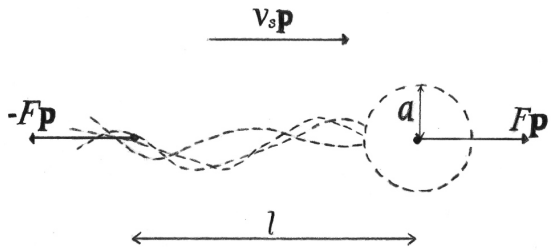

Figure 4.1 Schematic representation of a model pusher microswimmer.

4.1 Swimmer model

In our simulations, we consider N microswimmers moving through a fluid, represented by the Navier-Stokes equations as solved by a lattice Boltzmann solver, as explained in Section 4.2. Each of the swimmers is modelled as extended force dipoles, with the two point forces representing the propulsive force exerted by the (front- or rear-mounted) flagella. Since each swimmer is force free, the forces are equal in magnitude with opposite signs, $\pm F\mathbf{p}$, where $\mathbf{p}$ is the orientation of the swimmer and F is the magnitude of the force. The two forces are separated by a length l, which we use as the basic measure of the swimmer size. A schematic representation of the swimmer is shown in Fig. 4.1. The force dipole is characterized by the dipole strength κ as defined in Eq. 2.6, and the sign of κ determines the type of swimmer (pusher or puller). The position, $\mathbf{r}_i$, and orientation, $\mathbf{p}_i$, of swimmer i evolves according to the following equations of motion:[36,65]

$$\dot{\mathbf{r}}_i = v_s\mathbf{p}_i + \mathbf{U}(\mathbf{r}_i), \tag{4.1}$$

$$\dot{\mathbf{p}}_i = (\mathbb{I} - \mathbf{p}_i\mathbf{p}_i)\cdot\nabla\mathbf{U}(\mathbf{r}_i)\cdot\mathbf{p}_i \approx (\mathbb{I} - \mathbf{p}_i\mathbf{p}_i)\cdot\frac{\mathbf{U}(\mathbf{r}_i) - \mathbf{U}(\mathbf{r}_i - l\mathbf{p}_i)}{l} \tag{4.2}$$

where $\mathbf{U}(\mathbf{r}_i)$ is the fluid velocity evaluated at the position of the swimmer i, v_s is the constant swimming velocity, and $\mathbb{I}$ is the unit tensor. The discretized Jeffery's equation in Eq. 4.2 was used for an infinite aspect ratio. Jeffery's equation is used to describe the reorientation of a particle through a viscous medium. In addition to the reorientation described by Eq. 4.1 and 4.2, the microswimmers also undergo random reorientations with a frequency λ. This run-and-tumble motion results in a random walk, which has a persistence length $l_p = v_s/\lambda$.

Importantly, the microswimmers in this model have no explicitly resolved bodies, and are thus fully fore-aft symmetric apart from the self-propulsion added through Eq. 4.1. The introduction of this symmetry breaking can however be used to calculate

an "effective body size", assuming a spherical body of radius a in Fig. 4.1.[36] With no external velocity field present, one can write the force balance of the swimmer as:

$$F\mathbf{p} - 6\pi\mu a(v_s\mathbf{p} - \mathbf{W}) = 0 \tag{4.3}$$

where the second term on the left-hand side is the Stokes drag on the body, and $\mathbf{W}$ is the flow field generated by the flagellum evaluated at the head of the swimmer. This is given by a Stokeslet ($-F\mathbf{p}$) at the position of the flagellum, *i.e.*

$$\mathbf{W} = \frac{1}{8\pi\mu l}(\mathbb{I} + \mathbf{pp}) \cdot (-F\mathbf{p}) = -\frac{F\mathbf{p}}{4\pi\mu l}. \tag{4.4}$$

Substituting this into Eq. 4.3, one obtains the following expression for the swimming speed

$$v_s = \frac{F}{6\pi\mu a}\left(1 - \frac{3}{2}\frac{a}{l}\right). \tag{4.5}$$

The second term in Eq. 4.5 is a correction term to the Stokes–Einstein equation for an isolated spherical body. An effective radius a of the swimmer's body can be obtained from Eq. 4.5 in order to calculate approximate packing fractions that can be compared with experimental parameters.

4.2 Lattice Boltzmann method

To resolve the hydrodynamic interactions between microswimmers, the lattice Boltzmann (LB) method was used to solve the Navier–Stokes equations. It is based on the Boltzmann equation for molecules in a gas:[66]

$$\frac{\partial f}{\partial t} + u_\alpha \frac{\partial f}{\partial r_\alpha} + \frac{F_\alpha}{\rho}\frac{\partial f}{\partial u_\alpha} = \Omega(f) \tag{4.6}$$

where $f(\mathbf{r}, \mathbf{u}, t)$ is the phase-space density of particles with position $\mathbf{r}$ and momentum $\mathbf{u}$ at time t, and Ω is the so-called collision operator.

As indicated by its name, in the lattice Boltzmann method the distribution function at f is instead calculated at discrete points in space at discrete timesteps. Rather than representing individual fluid molecules, the fluid is thus described through these probability distributions; LB methods are therefore usually called "mesoscopic" methods.

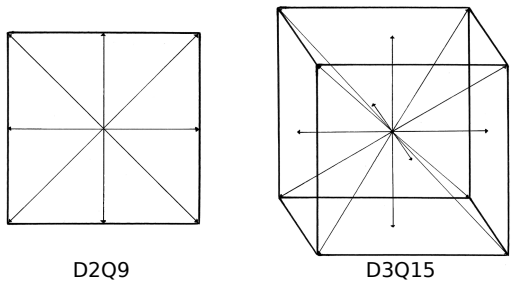

Figure 4.2 Schematic representation of a two- (left) and a three-dimensional LB lattice (right). The arrows show the set of velocity vectors $\mathbf{c}_i$.

Furthermore, the velocity directions are reduced to a finite set, where the number of possible directions depends on the lattice used. As an example, consider the two-dimensional lattice in Fig. 4.2 on the left, where the particle in the middle is able to move in 8 directions or remain at its original position. When the particle moves, it can do so with two different magnitudes for the velocity; 1 or $\sqrt{2}$, corresponding to moving along the axes or along the diagonals, respectively. We thus assign a discrete single-particle distribution function $f_i(x,t)$, where the index $i \in \{0,8\}$ represents the 9 possible velocity directions (including being stationary), to all lattice points. By calculating moments of the distribution functions f_i, one can then obtain the macroscopic observables of the fluid. The fluid density ρ can thus be expressed as

$$\rho = \sum_i f_i(\mathbf{r},t). \tag{4.7}$$

The fluid velocity is calculated as the average of the microscopic velocities:

$$\mathbf{U} = \frac{1}{\rho}\sum_i f_i(\mathbf{r},t)\mathbf{c}_i \tag{4.8}$$

where $\mathbf{c}_i$ is the velocity vector pointing in direction i. The velocities together with their weights form velocity sets that are indicated with DdQq, where d and q represent the dimension of the system and the number of accessible neighbouring lattice points, two examples are shown in Fig 4.2. One can discretize the Boltzmann equation (Eq. 4.6) to obtain the lattice Boltzmann equation:

$$f_i(\mathbf{r}+\mathbf{c}_i\Delta t, t+\Delta t) = f_i(\mathbf{r},t) + \Omega_i(\mathbf{r},t) \tag{4.9}$$

which describes the particle with a velocity $\mathbf{c}$ moving to the lattice point $\mathbf{r}+\mathbf{c}_i\Delta t$ during the time step Δt. Eq. 4.9 can conveniently be separated into alternating "streaming" steps, where the distribution functions are propagated along the lattice,

and "collision" steps, where the probability distributions are relaxed towards their local equilibrium value. The operator Ω_i can take on several forms and describes particle collisions in an approximate manner. A standard collision operator is the Bhatnagar–Gross–Krook (BGK) operator:[67]

$$\Omega_i(f) = -\frac{f_i - f_i^{eq}}{T}\Delta t. \tag{4.10}$$

The collision step redistributes the particles in phase space and relaxes the system towards equilibrium f_i^{eq}, where T is the relaxation time, and the equilibrium distribution is given by

$$f_i^{eq} = w_i \rho \left(1 + \frac{\mathbf{U}\cdot\mathbf{c}_i}{c_s^2} + \frac{(\mathbf{U}\cdot\mathbf{c}_i)^2}{2c_s^4} - \frac{\mathbf{U}\cdot\mathbf{U}}{2c_s^2}\right) \tag{4.11}$$

where w_i represents the weights of the velocity set, c_s is the speed of sound, relating pressure and density as $p = c_s^2\rho$. Combining Eqs. 4.9 and 4.10 we obtain the lattice Boltzmann equation with the BGK operator:

$$f_i(\mathbf{r} + \mathbf{c}_i\Delta t, t + \Delta t) = f_i(\mathbf{r}, t) - \frac{\Delta t}{T}\left(f_i(\mathbf{r}, t) - f_i^{eq}(\mathbf{r}, t)\right). \tag{4.12}$$

As described above, Eq. 4.12 can be thought of as a two-step process, where the right-hand side represents the effect of collisions, while the effect of these are then streamed to the neighbouring sites, as shown by the resulting distribution on the left-hand side.

4.3 Implementation of point forces

The lattice Boltzmann method, as described in Section 4.2, cannot directly be applied to systems with sedimenting particles, active matter, interacting polymers, etc., since it only contains the normally encountered pressure and viscous forces. To also include external forces such as gravity or the forces exerted by swimmers, one needs to implement such forces into the lattice Boltzmann scheme. Unlike gravity, which would add a spatially constant force over the surface of the particle in colloidal systems, it is often possible to approximate the effect of a particle with a point force, at least for distances that are large compared to the size of the particle. The implementation of such a model has been described by[68] where the singular forces at the position of the colloidal particles were regularized over two lattice units in each dimension, using a method by Peskin.[69] This scheme enables the interpolation of forces and fluid velocities between the off-lattice swimmers and the lattice fluid. The method introduces a new set of distribution functions

$$\bar{f}_i(\mathbf{r}, t) = f_i(\mathbf{r}, t) - \frac{\Delta t}{2}R_i(\mathbf{r}, t) \tag{4.13}$$

in which the propagation of the system can be written

$$\bar{f}_i(\mathbf{r}+\mathbf{c}_i\Delta t, t+\Delta t) = \bar{f}_i(\mathbf{r},t) + R_i(\mathbf{r},t)\Delta t \tag{4.14}$$

where $R_i = -\Omega_{ij}[f_j(\mathbf{r},t) - f_j^{eq}(\mathbf{r},t)] + \Phi_i(\mathbf{r},t)$ describes the forces and the collisions, where

$$\Phi_i(\mathbf{r},t) = w_i\left(\frac{\mathbf{F}\cdot\mathbf{c}_i}{c_s^2} + \frac{(\mathbf{UF}+\mathbf{FU}):\mathbb{Q}_i}{2c_s^4}\right). \tag{4.15}$$

Here, $\mathbb{Q}_i = \mathbf{c}_i\mathbf{c}_i - c_s^2\mathbb{I}$ and $\mathbf{F}$ is the force acting on the lattice point. The latter is obtained by interpolating all swimmer forces using the regularized δ-function[69]

$$\delta^p(\mathbf{r}) = \frac{1}{(\Delta L)^3} g\left(\frac{x}{\Delta L}\right) g\left(\frac{y}{\Delta L}\right) g\left(\frac{z}{\Delta L}\right) \tag{4.16}$$

$$g(r) = \begin{cases} \frac{3-2|r|+\sqrt{1+4|r|-4r^2}}{8}, & |r| \le 1, \\ \frac{5-2|r|-\sqrt{-7+12|r|-4r^2}}{8}, & 1 \le |r| \le 2, \\ 0, & |r| \le 2 \end{cases} \tag{4.17}$$

where ΔL is the lattice spacing. With this regularization, one can also easily represent an extended dipole, like the one used in this thesis, as a combination of two point forces having the same magnitude, a distance l apart.

4.4 Computational details

The D3Q15 lattice (as in Fig. 4.2) was used with periodic boundary conditions for the 3-dimensional simulations, while in quasi-2 dimensions, no-slip walls were applied in the z direction. In LB units, we used $F = 1.57 \times 10^{-3}$, $l = 1$, $\mu = 1/6$ and $\lambda = 2\times10^{-4}$, and if not specified otherwise, $v_s = 10^{-3}$. The results are presented in nondimensionalized units, where the lengthscales are scaled with the swimmer size l and the timescales with l/v_s. These numbers were chosen to ensure the low Reynolds number limit, which yields $\mathrm{Re} = 6\times10^{-3}$. We can compare the nondimensionalized dipole strength $\kappa_n = F/(\mu l v_s) \approx 9.4$ with the same value for an *E. coli*, which is $\kappa_n \approx 11.2$ using $F = 0.42$ pN and $l = 1.9\ \mu$m[70].

5 Active turbulence in three dimensions

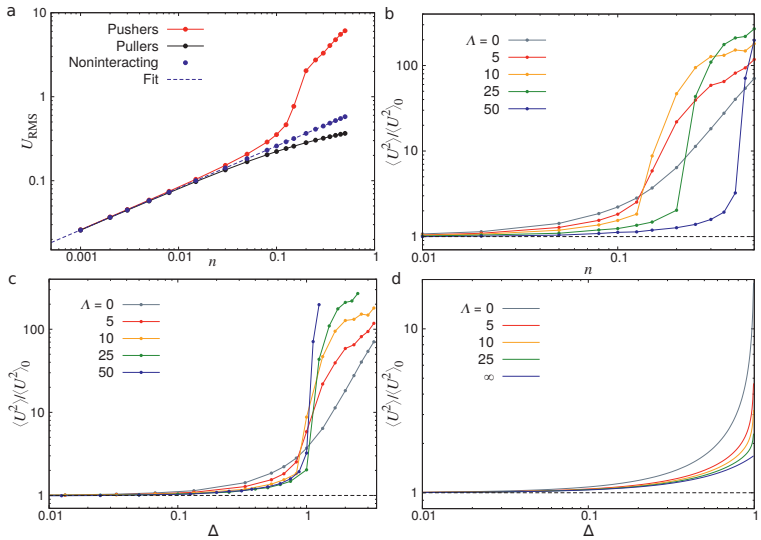

Figure 5.1 (a) The root-mean-square fluid velocity as a function of swimmer density for pushers, pullers and noninteracting swimmers, in a simulation box of $L = 150$ and $v_s = 0.001$. In (b, c, d) the fluid velocity variance $\langle U^2\rangle$ divided by the corresponding noninteracting value $\langle U^2\rangle_0$ is plotted for different reduced persistence lengths $\Lambda = v_s/(\lambda l)$. In (b) it is plotted as a function of swimmer density n and in (c, d) as a function of $\Delta = n/n_c$, obtained from (c) LB simulations and (d) from kinetic theory. The dashed line represents the noninteracting case.

In this chapter, the main results of Papers I and II are summarized, where both the transition to active turbulence and the ensuing collective state was characterized. In Paper II, we studied the effect of the swimming speed on the transition to collective motion. Using a three-dimensional simulation box and a large number of swimmers enabled us to determine the emerging length- and timescales of the collective behaviour.

We first investigated the root-mean-square (RMS) fluid velocity, $U_{RMS} = \langle U^2\rangle^{1/2}$, as a function of the microswimmer number density $n = N/L^3$ for pushers, pullers and noninteracting microswimmers, while keeping the swimming speed constant at $v_s = 0.001$. Noninteracting swimmers constitute a reference model, where all interactions between the swimmers are switched off, while they are still swimming with a constant velocity and stirring up the surrounding fluid, corresponding to Eqs. 4.1 and 4.2 with all terms containing $\mathbf{U}$ removed. The results of these simulations for the different types of swimmers are shown in Fig. 5.1a. It is clear that at very low densities, swimmer–swimmer interactions are negligible, and pushers and pullers become statistically equivalent. When increasing the density of swimmers, U_{RMS} increases proportionally to $n^{1/2}$, in accordance with previous results.[36] With increasing density, pushers and pullers begin to deviate from the noninteracting swimmer results, although in different ways. As discussed in Chapters 2.2 and 3.1, pullers have a

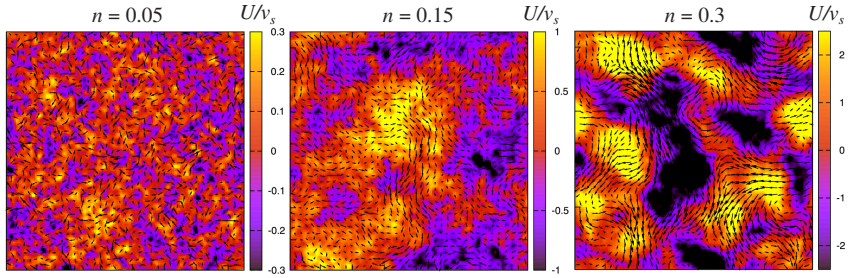

Figure 5.2 Snapshots of the fluid velocity field at different microswimmer densities. The arrows show the fluid velocities in the xy plane while the colours show the velocities in the third dimension.

different single-swimmer flow field compared to pushers and they do not show any collective behaviour in three dimensions. In accordance with this, the RMS fluid velocity curve for pullers falls below the one for noninteracting swimmers. For pushers, however, the RMS fluid velocity increases dramatically beyond a density of $n \approx 0.15$ indicating a transition to collective motion. This development of collective motion is clearly visible in Fig. 5.2, which shows snapshots of the fluid velocity field for pusher suspensions. Consequently, we mostly focused on pushers in the projects described in Papers I and II.

As we can see from Eq. 5.3, the critical density is not affected by the swimming speed, and previous studies[4,36] have already shown that that bacterial turbulence is still present for shakers, where $v_s = 0$, even though the effect of the swimming speed on the transition remains to be investigated. Recent results from kinetic theory[52] furthermore predict that swimmer–swimmer correlations are important even far below the transition to collective motion. However, unlike the transition to bacterial turbulence, these pretransitional correlations are predicted to be suppressed by swimming, making the transition curve steeper. In Paper II, we compare simulation results below the transition to a number of predictions from kinetic theory. We furthermore studied the effect of swimming speed *above* the transition, a regime, which is not accessible using kinetic theory. We varied the swimming speed v_s, which we quantify through the non-dimensional microswimmer persistence length $\Lambda = v_s/(\lambda l)$. The tumbling frequency was kept constant at the same value as in Paper I, in order to keep a constant value of the critical density n_c. The values used can be found in Table 5.1. However, as one can see from Table 5.1, the critical density moves to higher values for the two highest swimming velocities considered ($\Lambda = 25$ and $\Lambda = 50$). This is not in accordance with theoretical predictions, but can be explained by the presence of inertial effects in the LB simulations, which become significant at high swimming velocities. In order to account for this and to be able to compare the curves both directly and to the predictions from kinetic theory, we plot the fluid velocity variance $\langle U^2 \rangle$

Table 5.1 Swimming velocity v_s used in the simulations and the corresponding values of the reduced persistence length. The values of the observed critical density n_c are also shown together with the corresponding values of Δ at $n = 0.1$ in order to compare the simulation results with kinetic theory.

v_s	Λ	n_c	$\Delta(n = 0.1)$
0	0	0.15	0.7
0.001	5	0.15	0.7
0.002	10	0.15	0.7
0.005	25	0.2	0.5
0.01	50	0.4	0.3

for different values of Λ against the rescaled density $\Delta = n/n_c$, where the n_c values used can be found in Table 5.1. All sufficiently low densities, all pusher suspensions in Fig. 5.1b behave like noninteracting ones (dashed line), but one can see that the deviation from noninteracting behaviour gets smaller as Λ is increased, indicating a suppression of swimmer-swimmer correlations for higher swimming velocities. As a comparison, the theoretical predictions [52] below the transition are plotted in Fig. 5.1c showing a good correspondence with our LB simulation data.

In order to find the characteristic length- (ξ) and timescales (τ) of the collective behaviour, the decay of the correlation of the fluid velocity was calculated. The spatial and temporal velocity correlation functions are defined as:

$$c(R) = \langle \mathbf{U}(\mathbf{0}) \cdot \mathbf{U}(\mathbf{R}) \rangle \tag{5.1}$$

$$c(t) = \langle \mathbf{U}(0) \cdot \mathbf{U}(t) \rangle \tag{5.2}$$

In Fig. 5.3a, the spatial velocity correlation function of the fluid velocity in pusher suspensions at four different densities and $\Lambda = 5$ is shown. The velocity correlations decay quickly at low densities but becomes significantly more long-ranged in the transition region and in the collective motion regime. The same behaviour is seen when looking at the time correlation of the fluid velocity in Fig. 5.3b. To determine the characteristic length- and timescales of the bacterial turbulence, the value of r and t were determined when the correlation functions had decayed to 0.2 for the spatial correlation (dashed line in Fig. 5.3a) and 0.4 for the time correlation functions (Fig. 5.3b). Both the characteristic length- and timescales in Fig. 5.3c show peaks around the transition density $n = 0.15 - 0.2$ before decaying to a plateau value. As the location of the peaks in ξ and τ roughly correspond to the transition to active turbulence, we furthermore used this data to test previous predictions from kinetic theory for the value of the critical density n_c for the onset of collective motion. The critical density required for the transition to bacterial turbulence in an infinite,

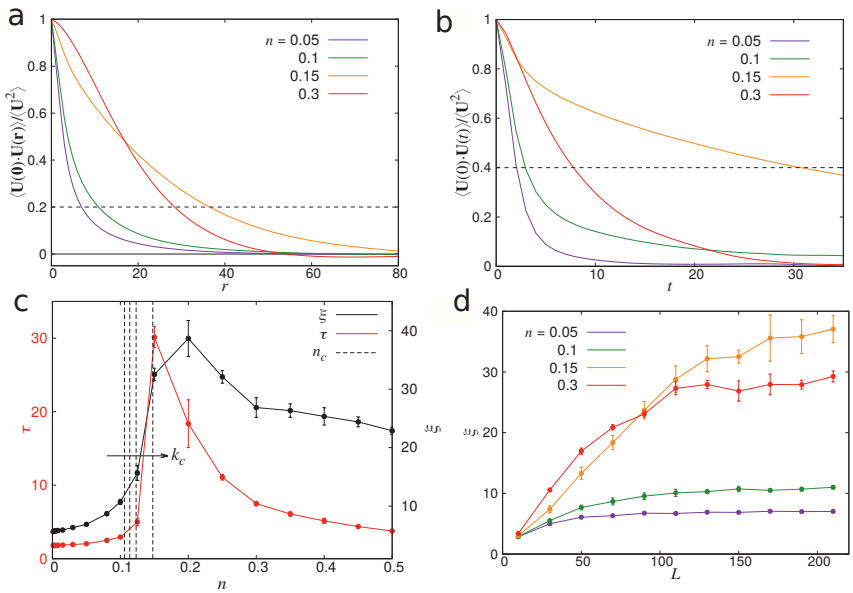

Figure 5.3 (a) Spatial and (b) time correlation functions of the fluid velocity for a system with $L = 210$ and $v_s = 0.001$ (corresponding to $\Lambda = 5$). The dashed line shows the value used to determine the characteristic length- and timescales. (c) The characteristic length- (ξ) and timescales (τ) for $L = 150$. The dashed lines indicate the critical densities (n_c) obtained with different wavevectors, k_c. (d) The characteristic lengthscale for different densities as a function of the box length L show the finite size effects. The error bars were obtained by subdividing each simulation into blocks.

unbounded suspension, n_c is given by[12,36,49-51]

$$n_c = 5\lambda/\kappa \tag{5.3}$$

For the parameters used in this work, this corresponds to a critical density of $n_c = 0.106$. This is somewhat lower than the transition density as estimated from the simulations. Kinetic theory shows, that, in three dimensions, the instability occurs at the largest lengthscale available to the system, corresponding to the critical wavevector $k_c \to 0$. In a simulation, the critical density will, however, change due to the finite box and the hydrodynamic screening is introduced by the use of periodic boundary conditions (PBCs). We numerically calculated the critical density for different wavevectors up to $k_c = 8\pi/L$.[51,65] As can be seen in Fig. 5.3c, the result using the highest wavevector matches the simulation results indicating, that the shift of the transition density is at least partially a finite-size effect. Using the length- and timescales, we could also estimate the typical size of the simulation box necessary, to avoid excessive finite size effects. The lengthscales in Fig. 5.3d seem to reach a plateau above $L = 100$ for the data in both the transition ($n = 0.15$) and collective

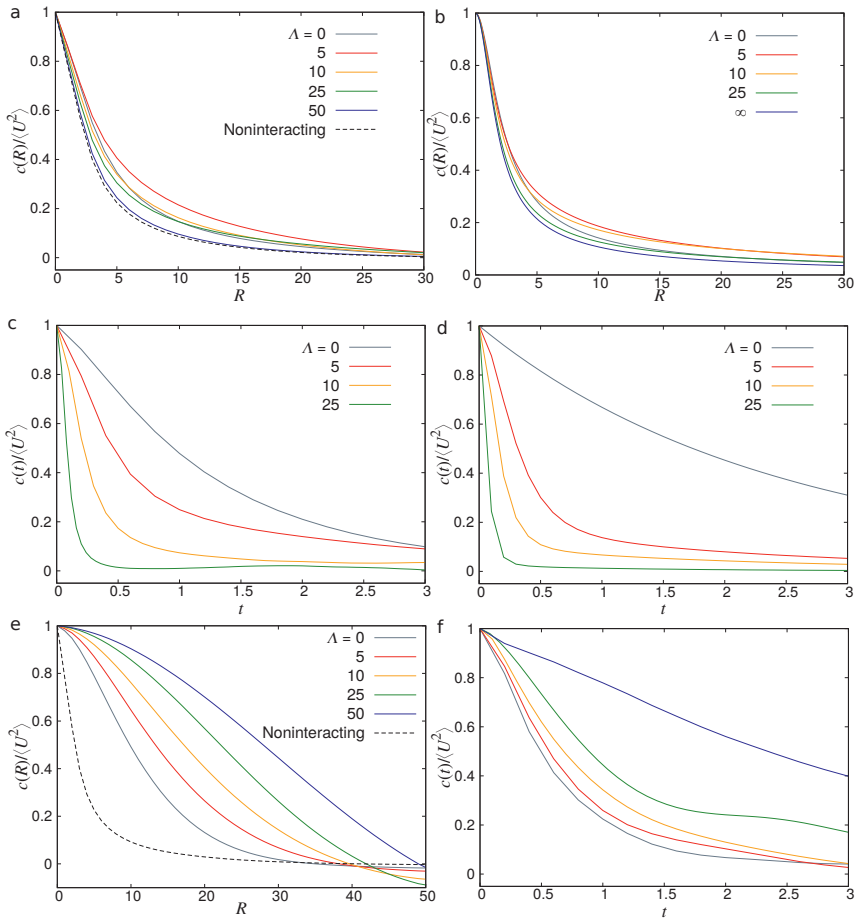

Figure 5.4 (a) The spatial velocity correlation functions below the transition ($n = 0.1$) from (a) LB simulations and (b) kinetic theory, together with the temporal correlations below the transition for (c) LB simulations and (d) kinetic theory. The spatial (e) and temporal (f) correlations are also plotted above the transition ($n = 0.5$) from LB simulations. Here, the colours are the same as in (e).

region ($n = 0.3$). This shows that large-scale simulations (minimum 10^5 particles) are needed to study collective motion in bacterial suspensions.

The spatial and time correlation functions were also investigated for different swimming speeds (Fig. 5.4). In panels a and b, the velocity correlation functions are plotted, obtained from LB simulations and from kinetic theory,[52] respectively. With increasing Λ the correlations come closer to the data for the noninteracting system, where there are no swimmer–swimmer correlations confirming the qualitative picture from the fluid velocity variance data (Fig 5.1). The simulation results are in good

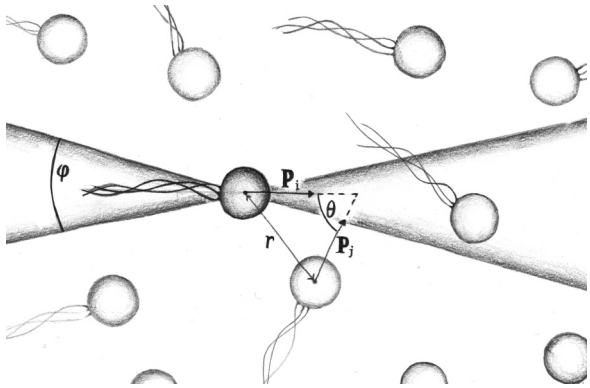

Figure 5.5 The angle θ between the orientations of two swimmers separated by a distance r.

agreement with the predictions from kinetic theory (Fig, 5.4b). Looking at the time correlations (Fig. 5.4c and d), the trend is the same for both LB and kinetic theory results: the correlation decreases faster with increasing Λ. There is a quantitative difference for shakers ($\Lambda = 0$) between the two data sets, which could be due to the approximated values of n_c when calculating Λ for the simulations, or the finite size effect when using a simulation box. Kinetic theory cannot predict the behaviour above the critical density, so only simulation results are available for both correlation functions (Fig. 5.4e and f). The spatial correlations in the collective regime ($n = 0.5$) increase monotonically with Λ, which means that the characteristic lengthscales of the turbulent flow increase with increasing swimming velocity. The time correlations also increase with Λ, which is the opposite behaviour compared to the case below the transition. Surprisingly, this means that the timescale increases with increasing v_s, corresponding to a "slowing down" of the collective flows with faster swimming.

We now turn to characterize the behaviour of the swimmers. In three dimensions, we find no sign of any density inhomogeneity for the swimmers. In agreement with previous studies [12,36,50,51] we find that the transition to bacterial turbulence is completely due to the mutual reorientation of the pusher swimmers. In order to quantify this, we looked at the orientational ordering of the swimmers. Defining the angle θ between the orientation of two swimmers separated by a distance r (Fig 5.5), the polar $P(r)$ and nematic order parameters $S(r)$ were defined as

$$P(r) = \langle P_1(\cos\theta)\rangle_{|\mathbf{r}_i - \mathbf{r}_j| = r} = \langle \cos\theta \rangle_r \tag{5.4}$$

and

$$S(r) = \langle P_2(\cos\theta)\rangle_{|\mathbf{r}_i - \mathbf{r}_j| = r} = \left\langle \frac{3\cos^2\theta - 1}{2} \right\rangle_r \tag{5.5}$$

where P_1 and P_2 are the first and second Legendre polynomials.

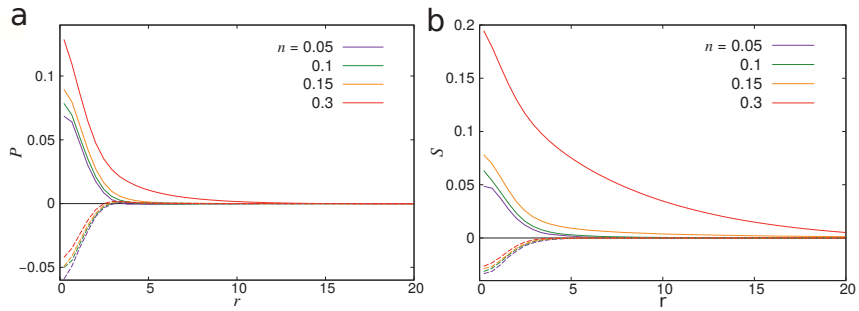

Figure 5.6 (a) The polar order parameter $P(r)$ and (b) the nematic order parameter $S(r)$ of the swimmers at different densities. Solid lines indicate pushers and dashed lines represent pullers.

It is clear from Fig. 5.6a that there is a weak local polar alignment for pushers (solid lines) and antialignment for pullers (dashed lines). Both of them converge to zero around $r = 5$. In the case of the nematic order parameter in Fig. 5.6b, there is antialignment for the pullers (dashed lines), but for pushers there is a significant ordering at the highest density, which corresponds to the collective region. This indicates that the transition to active turbulence is driven by the local nematic order induced by hydrodynamic interactions, which is in accordance with previous theoretical predictions[52]. This correlation is also more long-ranged than the polar ordering and decays towards zero only above $r = 20$. These results show that the far-field hydrodynamics is enough to cause significant nematic ordering of the swimmers even in the absence of direct collisions between the swimmers, which are, however, likely to strengthen this ordering. To compare with the lengthscale determined from the fluid statistics, we further characterized this by integrating the order parameters, in analogy with the Kirkwood G-factor, which measures the local orientational order in polar fluids:[71]

$$G_P(R) \equiv \int_0^R P(r) 4\pi n r^2 dr, \tag{5.6}$$

$$G_S(R) \equiv \int_0^R S(r) 4\pi n r^2 dr. \tag{5.7}$$

The functions G_P and G_S measure the range of the polar and nematic ordering, respectively, around a single swimmer. Using the curves in Fig. 5.7a we define the lengthscales ξ_P and ξ_S as the maximum of the corresponding $G(R)$ curves. We can now compare the lengthscale determined from the swimmers in Fig. 5.7b with our previous results for the fluid velocity. The shape of the curves is similar to those in Fig. 5.3b, but there are quantitative differences in the ξ-values. In the case of ξ_P, this could be due to the arbitrary cutoff used when analysing the spatial correlation functions. The ξ_S curve, however, is shifted to higher values and with larger statistical fluctuations, in accordance with the long-ranged nematic ordering in Fig. 5.6b.

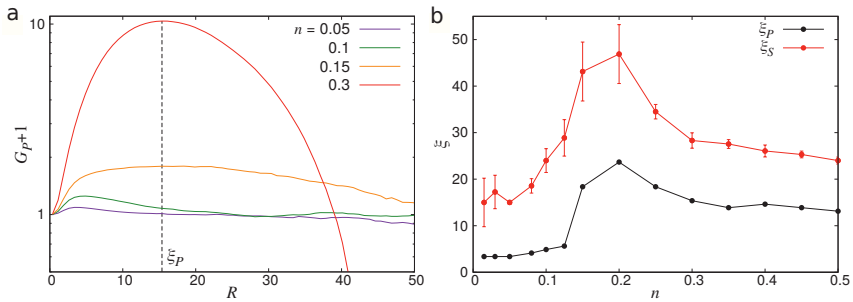

Figure 5.7 Characteristic lengthscales measured from the local polar and nematic ordering of the swimmers. The cumulative polar order, G_P, (a) and the resulting lengthscales (b). The error bars were obtained by subdividing the simulations into four equal time intervals.

Nevertheless, we can conclude that all three methods used to obtain the characteristic lengthscales in bacterial turbulence yield a maximum around the transition density and go to a finite value in the collective regime, although the precise values of ξ differ somewhat between the methods.

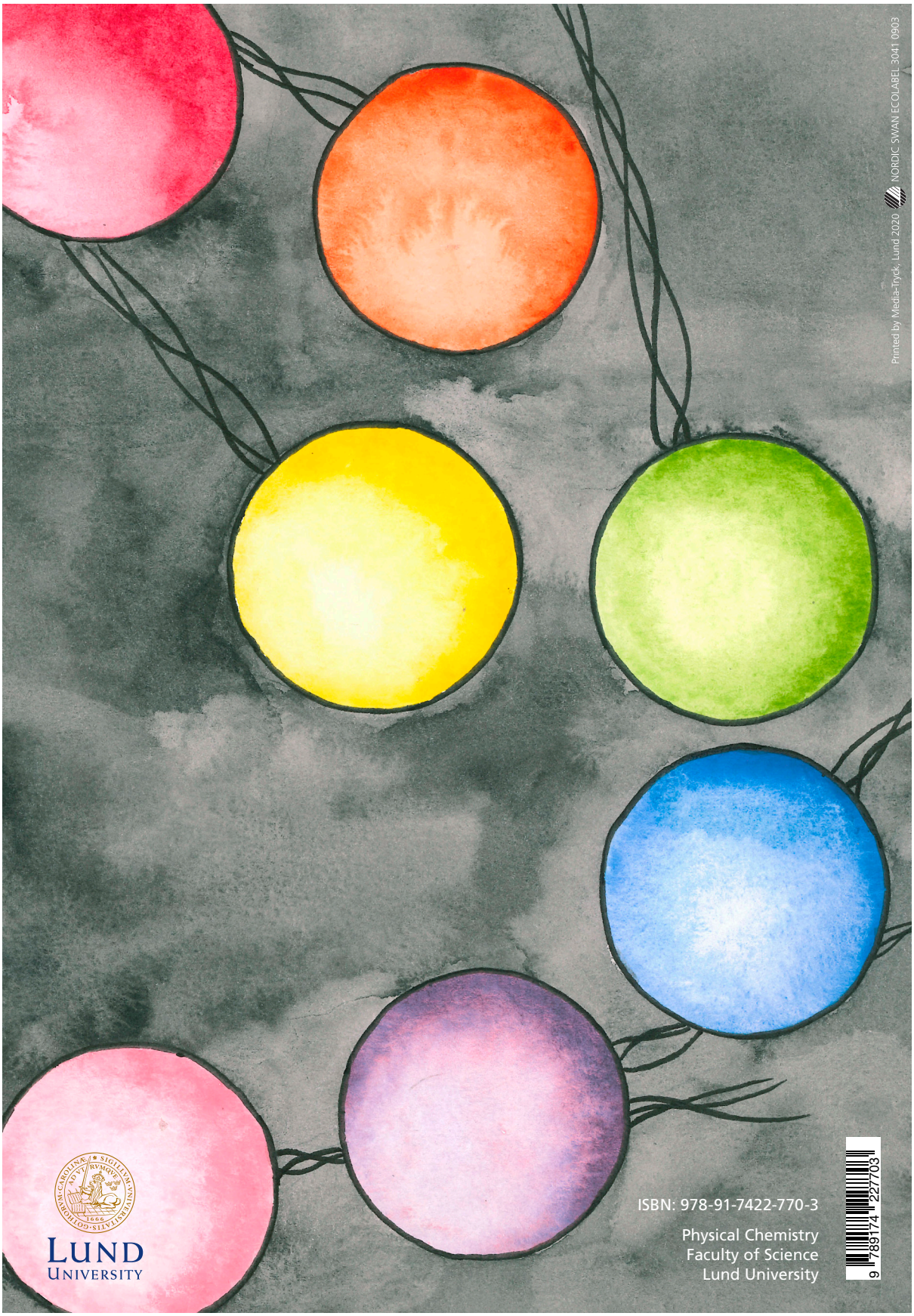

Printed by Media-Tryck, Lund 2020 NORDIC SWAN ECOLABEL 3041 0903

LUND UNIVERSITY

ISBN: 978-91-7422-770-3

Physical Chemistry
Faculty of Science
Lund University